# Return Mapping Algorithms and Stress Predictors for Failure Analysis in Geomechanics

Jinsong Huang[1] and D. V. Griffiths[2]

**Abstract:** Two well-known return mapping algorithms, the closest point projection method (CPPM) and the cutting plane algorithm (CPA), have been analyzed in detail in relation to two classical failure problems in geomechanics, namely, bearing capacity and slope stability. The stability and efficiency of the algorithms have been investigated in relation to two types of stiffness operators, namely, the consistent elastoplastic modulus and the continuum elastoplastic modulus, and two types of stresses prediction strategies, namely, path independent (based on stresses at previous step) and path dependent (based on stresses at the previous iteration). The numerical experiments show that CPPM working with a consistent elastoplastic modulus and a path independent strategy gives the best performance. It was also observed, however, that the CPA with a continuum elastoplastic modulus and path dependent strategy was quite stable and efficient. This latter observation has implications for advanced constitutive modeling since CPA with a continuum elastoplastic modulus avoids the need for evaluation of the second derivatives of the plastic potential function, making it easier to deal with complicated yield surfaces.

**DOI:** 10.1061/(ASCE)0733-9399(2009)135:4(276)

**CE Database subject headings:** Finite element method; Geotechnical engineering; Failures; Constitutive models; Elastoplasticity.

## Introduction

Iterations for finite-element analysis of material nonlinear can be, in general, separated into two levels. The first (local) level is tied to the constitutive equations where, for a given strain increment, the algorithm iterates in stress and internal variable space until a convergence criterion is met. The second (global) level involves iterations to achieve a balance of internal stresses with external loads. The techniques for integration of the constitutive equations at the local level directly control the accuracy and stability of the overall numerical solution. Generally speaking, these techniques fall into two categories, namely, explicit (forward Euler) and implicit (backward Euler). Explicit schemes (Nayak and Zienkiewicz 1972; Zienkiewicz et al. 1969; Owen and Hinton 1980) were widely employed until Simo and Taylor (1985) proposed the implicit closest point projection method (CPPM) which is a type of "return mapping" algorithm. The return mapping involves first integrating the elastic equations with total strain increments to obtain an elastic predictor. The elastically predicted stresses are then relaxed onto a suitably updated yield surface by correcting, iteratively, the plastic strain increments. The radial return method proposed by Krieg and Krieg (1977) is easily shown to be a special case of CPPM for von Mises plasticity.

Simo and Taylor (1985) showed that the CPPM with a consistent elastoplastic modulus (also referred to as the algorithmic stiffness; Jirasek and Bažant 2001) achieves an asymptotic global quadratic convergence rate when using the full Newton–Raphson method. The concept of consistent linearization was introduced by Hughes and Pister (1978) and consistent elastoplastic modulus was derived for viscoplasticity by Hughes and Taylor (1978). To construct the consistent elastoplastic modulus, the change of the stress evaluated by a special return mapping algorithm corresponding to an infinitesimal change of total strain increment is considered. It is different from the continuum elastoplastic modulus which is obtained by differentiation of the constitutive law.

The accuracy and stability of return mapping algorithms has been examined by Ortiz and Popov (1985). The asymptotic quadratic rate of convergence of CPPM makes the approach attractive, however there are three significant drawbacks. First, there is a practical difficulty in computation of the consistent tangent matrix when the return is nonradial. Second, the gradients of the plastic flow direction (second derivatives) are required leading to extra computing effort. Third, convergence of the local iterations can be a major issue for complex models (for instance, with highly nonlinear coupling between hardening or softening parameters). The third drawback is also found with relatively simple models (i.e., perfectly plastic models) at the Gauss points when stresses occur in zones of high curvature of the yield surface. In these cases the plastic corrector can have difficulties in returning to the yield surface. Numerical results reported in De Souza Neto et al. (1994), Bićanić and Pearce (1996), and Péréz-Foguet et al. (2001) illustrate some of these difficulties. Caddemi and Martin (1991) show that a line search algorithm must be included to ensure global convergence when CPPM is combined with the full Newton–Raphson method.

In order to improve convergence, Crisfield (1991) proposed a line search technique for the global iterations and Armero and Pérez-Foguet (2002); Pérez-Foguet and Armero (2002), and Jeremić (2001) even used a line search technique for the local iterations. For the Mohr–Coulomb failure surface, which is widely

[1]Assistant Research Professor, Division of Engineering, Colorado School of Mines, Golden, CO 80401. E-mail: jhuang@mines.edu

[2]Professor, Division of Engineering, Colorado School of Mines, Golden, CO 80401 (corresponding author). E-mail: d.v.griffiths@mines.edu

Note. Associate Editor: Arif Masud. Discussion open until September 1, 2009. Separate discussions must be submitted for individual papers. The manuscript for this paper was submitted for review and possible publication on May 29, 2007; approved on October 6, 2008. This paper is part of the *Journal of Engineering Mechanics*, Vol. 135, No. 4, April 1, 2009. ©ASCE, ISSN 0733-9399/2009/4-276–284/$25.00.

used in geomechanics, a closed-form return formula in principal stress can be employed, as described by Borja et al. (2003), Larsson and Runesson (1996), and Clausen et al. (2006). de Borst (1987) gave explicit return expressions using Koiter's method (Koiter 1953) along with a region indicator to deal with the singular yield points of the Mohr–Coulomb model. Crisfield (1997) employed a similar approach involving a two-vector return procedure. Huang and Griffiths (2008) compared five previously published algorithms for return mapping to Mohr–Coulomb in a finite-element analysis of bearing capacity.

A quite different return mapping approach that has received attention in the literature is the cutting plane algorithm (CPA) presented in Simo and Ortiz (1985) and Ortiz and Simo (1986). The method is based on a steepest descent strategy which avoids the need for an implicit treatment of the governing equations. The resulting scheme involves an explicit iterative process, thus exhibiting improved convergence properties. However, the lack of consistent linearization (Simo and Hughes 1998) in CPA methods limits their use in practical finite-element implementations employing a Newton–Raphson solution strategy. Simo (1998) reported that when using CPA, in contrast to CPPM, significant errors can result from the application of large load steps although no explanation was provided. In this paper, we will show that this problem with CPA can be overcome by the use of a path dependent strategy.

The effectiveness of two global stiffness operators, namely a consistent elastoplastic modulus and a continuum elastoplastic modulus working with the CPPM and CPA, along with two types of stress predictors, namely path dependent and path independent, are investigated in this paper. Numerical results of two classical geomechanics problems of bearing capacity and slope stability will show that the CPA working with a continuum elastoplastic modulus and stresses that are path dependent (based on previous iteration) is quite stable and efficient. The significant error observed by Simo (1998) for large load steps of CPA is found only when stresses are path independent (based on previous step). Furthermore, CPA with a continuum elastoplastic modulus avoids the need for evaluation of the second derivatives of the plastic potential function, making it easier to deal with complicated yield surfaces.

## Review of Standard Elastoplasticity

For simplification, we will restrict this paper to small strain, associated perfect plasticity.

The starting point for any small-strain elastoplastic relation is the fundamental split of the strain rate $\{\dot{\varepsilon}\}$ into an elastic component $\{\dot{\varepsilon}^e\}$ and a plastic component $\{\dot{\varepsilon}^p\}$

$$\{\dot{\varepsilon}\} = \{\dot{\varepsilon}^e\} + \{\dot{\varepsilon}^p\} \tag{1}$$

Based on this decomposition, the elastic stress-strain relationship can be rewritten as

$$\{\dot{\sigma}\} = [D^e](\{\dot{\varepsilon}\} - \{\dot{\varepsilon}^p\}) \tag{2}$$

where $[D^e]$ is the elastic stress-strain matrix.

Plastic strain rates for associated plasticity are assumed to follow the relations

$$\{\dot{\varepsilon}^p\} = \dot{\lambda}\{a\}, \quad \{a\} = \left\{\frac{\partial F}{\partial \sigma}\right\} \tag{3}$$

where $F$ is the yield and plastic potential function; $\dot{\lambda}$ is the consistency parameter, which represents the magnitude of the plastic flow and $\dot{\lambda} \geq 0$; $\{a\}$ is the flow direction, which is obtained upon differentiation of the plastic potential function with respect to stress. The use of an associated flow rule ensures that the plastic strain-increments are vectors perpendicular to the potential surface.

Loading-unloading conditions can be stated as

$$\dot{\lambda} \geq 0, \quad F \leq 0, \quad \dot{\lambda}F = 0 \tag{4}$$

which are sometimes referred to Kuhn–Tucker conditions. The first of these indicates that the consistency parameter is nonnegative while the second indicates that the stress states must lie on or within the yield surface. The last condition assures that the stresses lie on the yield surface during plastic loading.

From the loading-unloading conditions, it is easy to state the consistency condition as

$$\dot{\lambda}\Delta F = 0, \quad \text{if } F = 0 \tag{5}$$

hence, if $\dot{\lambda} \neq 0$, then $\Delta F = 0$, that is to say

$$\{a\}^T\{\dot{\sigma}\} = 0$$

$$\{a\}^T[D^e](\{\dot{\varepsilon}\} - \{\dot{\varepsilon}^p\}) = 0$$

$$\{a\}^T[D^e](\{\dot{\varepsilon}\} - \dot{\lambda}\{a\}) = 0$$

$$\dot{\lambda} = \frac{\{a\}^T[D^e]\{\dot{\varepsilon}\}}{\{a\}^T[D^e]\{a\}} \tag{6}$$

Note that $\{a\}$ is dependent on the stress state which is dependent on $\dot{\lambda}$ through Eq. (3), so Eq. (6) is a nonlinear equation.

Substituting Eq. (6) into the first of Eqs. (3), we have

$$\{\dot{\varepsilon}^p\} = \frac{\{a\}^T[D^e]\{\dot{\varepsilon}\}}{\{a\}^T[D^e]\{a\}}\{a\} \tag{7}$$

Substituting Eq. (7) into Eq. (2)

$$\{\dot{\sigma}\} = [D^{ep}]\{\dot{\varepsilon}\} \tag{8}$$

where $[D^{ep}]$ is the continuum elastoplastic modulus given by

$$[D^{ep}] = [D^e] - \frac{[D^e]\{a\}\{a\}^T[D^e]}{\{a\}^T[D^e]\{a\}} \tag{9}$$

## Closest Point Projection Method

### Iteration Procedure

In the CPPM method, the increments of plastic strain calculated at the end of the step and the yield condition is enforced at the end of the step, thus the integration scheme is written as

$$\{\varepsilon_{n+1}\} = \{\varepsilon_n\} + \{\Delta\varepsilon\} \tag{10}$$

$$\{\varepsilon^p_{n+1}\} = \{\varepsilon^p_n\} + \Delta\lambda_{n+1}\{a_{n+1}\} \tag{11}$$

$$\{\sigma_{n+1}\} = [D^e](\{\varepsilon_{n+1}\} - \{\varepsilon^p_{n+1}\}) \tag{12}$$

$$F_{n+1} = F(\{\sigma_{n+1}\}) = 0 \tag{13}$$

Given the set $(\{\varepsilon_n\},\{\varepsilon_n^p\},\{\Delta\varepsilon\})$ at step $n$, because $\{\sigma_{n+1}\}$ is dependent on $\Delta\lambda_{n+1}$, equations from Eqs. (10)–(13) are a set of nonlinear algebraic equations in $(\{\sigma_{n+1}\},\{\varepsilon_{n+1}^p\})$.

The strain $\{\varepsilon_{n+1}\}$ is obtained from the solution of the system of equations at step $n+1$. If the stresses are predicted based on the previous load step, it is understood that $\{\varepsilon_{n+1}\}$ is the total strain after the last iteration of the implicit solution scheme.

First note that from Eq. (11), the plastic strain increment is given by

$$\{\Delta\varepsilon_{n+1}^p\} = \{\varepsilon_{n+1}^p\} - \{\varepsilon_n^p\} = \Delta\lambda_{n+1}\{a_{n+1}\} \tag{14}$$

Substituting this expression into Eq. (12) gives

$$\begin{aligned}\{\sigma_{n+1}\} &= [D^e](\{\varepsilon_{n+1}\} - \{\varepsilon_n^p\} - \{\Delta\varepsilon_{n+1}^p\}) \\ &= [D^e](\{\varepsilon_{n+1}\} - \{\varepsilon_n^p\} - \Delta\lambda_{n+1}\{a_{n+1}\}) \\ &= [D^e](\{\varepsilon_n\} + \{\Delta\varepsilon\} - \{\varepsilon_n^p\} - \Delta\lambda_{n+1}\{a_{n+1}\}) \\ &= [D^e](\{\varepsilon_n\} - \{\varepsilon_n^p\}) + [D^e]\{\Delta\varepsilon\} - \Delta\lambda_{n+1}[D^e]\{a_{n+1}\} \\ &= \{\sigma_{n+1}^{\text{trial}}\} - \Delta\lambda_{n+1}[D^e]\{a_{n+1}\}\end{aligned} \tag{15}$$

where $\{\sigma_{n+1}^{trial}\}=\{\sigma_n\}+[D^e]\{\Delta\varepsilon\}$ is the trial stress of the elastic predictor and $-\Delta\lambda_{n+1}[D^e]\{a_{n+1}\}$ is the plastic corrector which returns or projects the trial stress onto the yield surface along a direction specified by the plastic flow direction at the endpoint. The elastic-predictor phase is driven by the increment in total strain while the plastic-corrector phase is driven by the plasticity parameter $\Delta\lambda_{n+1}$. Thus, during the elastic-predictor stage, the plastic strain remains fixed, and during the plastic-corrector stage, the total strain is fixed. If the normality rule is enforced at the end of the step, we have

$$\{\Delta\sigma_{n+1}\} = -[D^e]\{\Delta\varepsilon_{n+1}^p\} = -\Delta\lambda_{n+1}[D^e]\{a_{n+1}\} \tag{16}$$

The solution of the set of nonlinear Eqs. (10)–(13) based on the concept of closest point projection is typically obtained by a Newton procedure involving a systematic linearization. This results in a plastic corrector returning stresses to the yield surface. During the plastic-corrector stage of the algorithm, the total strain is constant and linearization is with respect to the increment $\Delta\lambda$ of the plasticity parameter.

As an example, in order to linearize an equation, $g(\Delta\lambda)=0$, using the Newton procedure with $\Delta\lambda^{(0)}=0$, at the $k$th iteration we would write

$$g^{(k)} + \left(\frac{dg}{d\Delta\lambda}\right)^{(k)} \delta\lambda^{(k)} = 0 \quad \Delta\lambda^{(k+1)} = \Delta\lambda^{(k)} + \delta\lambda^{(k)} \tag{17}$$

where $\delta\lambda^{(k)}$ is the increment in $\Delta\lambda$ at the $k$th iteration. For the sake of clarity, we will usually omit the load subscript $n+1$; thus, unless indicated otherwise, all quantities are evaluated at step $n+1$.

We write the plastic updates and yield condition in the form of Eq. (18), suitable for Newton iteration, thus defining $\{r\}$ as

$$\{r\} = -\{\varepsilon^p\} + \{\varepsilon_n^p\} + \Delta\lambda\{a\} = 0$$

$$F = F(\{\sigma\}) = 0 \tag{18}$$

linearization of these equations gives

$$\{r^{(k)}\} + [D^e]^{-1}\{\Delta\sigma^{(k)}\} + \Delta\lambda^{(k)}\{\Delta a^{(k)}\} + \delta\lambda^{(k)}\{a^{(k)}\} = 0$$

$$F^{(k)} + \{a^{(k)}\}^T\{\Delta\sigma^{(k)}\} = 0 \tag{19}$$

where

$$\{\Delta a^{(k)}\} = \left[\frac{\partial a^{(k)}}{\partial\sigma}\right]\{\Delta\sigma^{(k)}\} \tag{20}$$

Eqs. (19) are a set of two equations which can be solved for $\{\Delta\sigma^{(k)}\}$ and $\delta\lambda^{(k)}$. Substituting Eq. (20) into the first of Eqs. (19)

$$\{\Delta\sigma^{(k)}\} = -[R^{(k)}]\{r^{(k)}\} - \delta\lambda^{(k)}[R^{(k)}]\{a^{(k)}\} \tag{21}$$

where

$$[R^{(k)}] = \left[[\mathrm{I}] + \Delta\lambda^{(k)}[D^e]\left[\frac{\partial a^{(k)}}{\partial\sigma}\right]\right]^{-1}[D^e] \tag{22}$$

and substituting Eq.(21) into the second of Eqs. (19) and solving for $\delta\lambda^{(k)}$ we get

$$\delta\lambda^{(k)} = \frac{F^{(k)} - \{a^{(k)}\}^T[R^{(k)}]\{r^{(k)}\}}{\{a^{(k)}\}^T[R^{(k)}]\{a^{(k)}\}} \tag{23}$$

Thus, the update of the plastic strain and the plasticity parameter is

$$\{\varepsilon^{p(k+1)}\} = \{\varepsilon^{p(k)}\} + \{\Delta\varepsilon^{p(k)}\} = \{\varepsilon^{p(k)}\} - [D^e]^{-1}\{\Delta\sigma^{(k)}\}$$

$$\Delta\lambda^{(k+1)} = \Delta\lambda^{(k)} + \delta\lambda^{(k)} \tag{24}$$

With the increments as given in Eqs. (21) and (23), the Newton procedure is continued until convergence to the updated yield surface is achieved to within a sufficient tolerance.

It can be seen from Eq. (10) that CPPM is inherently path independent. If the stresses are predicted based on the previous iteration we have

$$\{\sigma^{(k+1)}\} = \{\sigma^{(k)}\} + [D^e]\{\Delta\varepsilon_{n+1}^{(i)}\} \tag{25}$$

where $i$ is the global iteration counter, $\{\sigma^{(k)}\}$ is the convergent value of stress at the local iteration, and $\{\Delta\varepsilon_{n+1}^{(i)}\}$ is the strain increment predicted using a global stiffness operator such as the consistent or continuum elastoplastic modulus.

The complete stress update algorithm (Belytschko et al. 2000) is given in Appendix I. Stress return terms corresponding to CPPM is shown in Fig. 1.

## Review of Consistent Elastoplastic Moduli

The consistent elastoplastic modulus for the CPPM is defined as

$$[D^{\text{epc}}] = \left(\frac{d\sigma}{d\varepsilon}\right)_{n+1} \tag{26}$$

To derive an expression for the consistent elastoplastic modulus, we write Eqs. (10)–(13) in incremental form (again dropping the subscripts $n+1$) as

$$\{d\sigma\} = [D^e](\{d\varepsilon\} - \{d\varepsilon^p\}) \tag{27}$$

$$\{d\varepsilon^p\} = d(\Delta\lambda)\{a\} + \Delta\lambda\{da\} \tag{28}$$

$$dF = \{a\}^T\{d\sigma\} = 0 \tag{29}$$

where

$$\{da\} = \left[\frac{\partial a}{\partial\sigma}\right]\{d\sigma\} \tag{30}$$

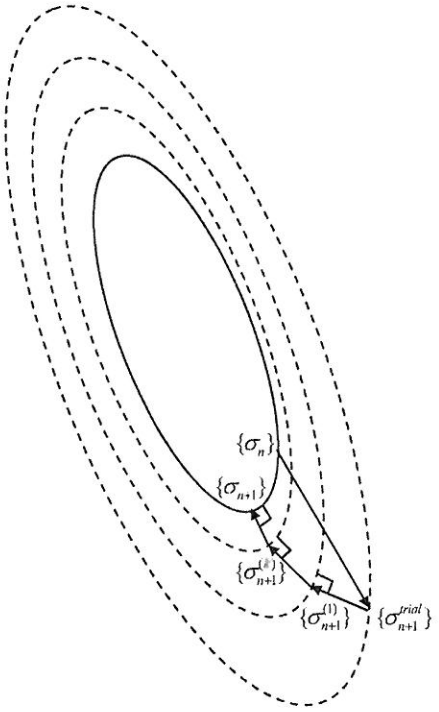


**Fig. 1.** Stress return corresponding to CPPM

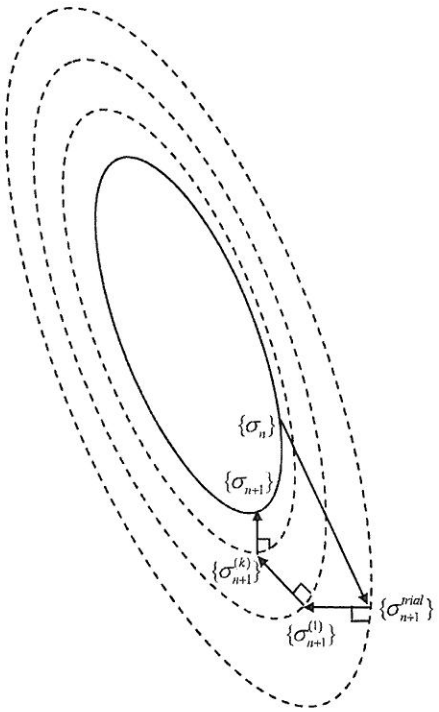


**Fig. 2.** Stress return corresponding to CPA

Substituting Eq. (28) into Eq. (27), using Eq. (30) and solving for $\{d\sigma\}$, we obtain

$$\{d\sigma\} = [R]\{d\varepsilon\} - d(\Delta\lambda)[R]\{a\} \tag{31}$$

where

$$[R] = \left[ [\mathrm{I}] + \Delta\lambda [D^e] \left[ \frac{\partial a}{\partial \sigma} \right] \right]^{-1} [D^e] \tag{32}$$

Substituting Eq. (31) into the incremental consistency condition [Eq. (29)] and solving for $d(\Delta\lambda)$ gives

$$d(\Delta\lambda) = \frac{\{a\}^T [R]\{d\varepsilon\}}{\{a\}^T [R]\{a\}} \tag{33}$$

Substituting this result into Eq. (31) we obtain

$$\{d\sigma\} = [D^{\mathrm{epc}}]\{d\varepsilon\} \tag{34}$$

where $[D^{\mathrm{epc}}]$ is the consistent elastoplastic modulus given by

$$[D^{\mathrm{epc}}] = [R] - \frac{[R]\{a\}\{a\}^T [R]}{\{a\}^T [R]\{a\}} \tag{35}$$

## Cutting Plane Algorithm

Using the same return mapping procedure as with CPPM, CPA is carried out by first integrating the elastic equations with total strain increments to obtain an elastic predictor. Then the elastically predicted stresses are relaxed onto a suitably updated yield surface by correcting iteratively the plastic strain increments. Following the same steps as used in Eq. (16), we get

$$\{\Delta\sigma^{(k)}\} = \{\sigma^{(k+1)}\} - \{\sigma^{(k)}\} = -[D^e]\{\Delta\varepsilon^{p(k)}\} \tag{36}$$

where $k$ is the iteration counter.

If the normality rule is enforced at the beginning of the iteration as in

$$\{\Delta\varepsilon^{p(k)}\} = \Delta\lambda^{(k)}\{a^{(k)}\} \tag{37}$$

substitution of Eq. (37) into Eq.(36) then gives

$$\{\Delta\sigma^{(k)}\} = -\Delta\lambda^{(k)}[D^e]\{a^{(k)}\} \tag{38}$$

At every iteration, if the yield function $F$ is linearized around the current values of stress $\{\sigma^{(k)}\}$, we get

$$F^{k+1} = F^k + \{a^{(k)}\}^T(\{\sigma^{(k+1)}\} - \{\sigma^{(k)}\}) \tag{39}$$

and substitution of Eq. (38) into Eq.(39), noting that $F^{k+1}=0$ gives

$$\Delta\lambda^{(k)} = \frac{F^{(k)}}{\{a^{(k)}\}^T [D^e]\{a^{(k)}\}} \tag{40}$$

It can be seen from Eq. (40) that CPA bypasses the need to compute the second derivatives as required by CPPM. However, the lack of consistent linearization (Simo and Hughes 1998) in CPA methods limits their use in practical finite-element implementations employing a Newton–Raphson solution strategy.

The complete stress update algorithm is given in Appendix II Stress return terms corresponding to CPA is shown in Fig. 2.

## Numerical Example Using CPPM

The stress update algorithm described in Appendix I is implemented in Program 6.5 from the open source finite-element codes of Smith and Griffiths (2004). Both the consistent and continuum elastoplastic modulus are considered. In order to demonstrate the different convergence rate for these two approaches under the full Newton–Raphson method, a footing problem has been analyzed as shown in Fig. 3. The mesh consists of 32 eight-noded elements. A denser mesh with 128 elements has been investigated and the

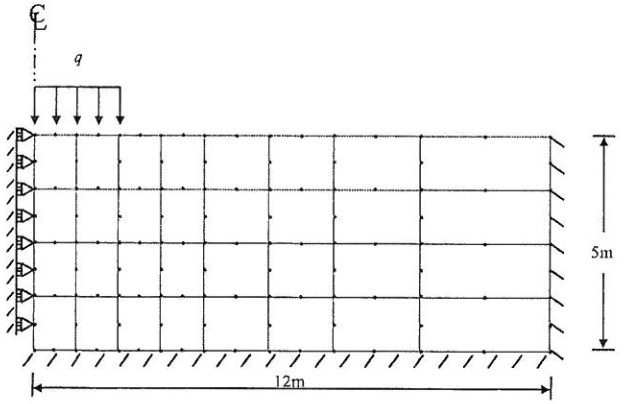


**Fig. 3.** Mesh of a strip footing

failure load along with the iteration number did not change significantly. To avoid overly stiff response, "reduced" 4 Gauss-points integration was used. Xia and Masud (2006) applied the stabilized mixed method (Masud and Xia 2005) to a three-surface elastoplastic cap model and got stable results in the full range of deformation for a similar footing problem. The analysis is of the "Prandtl problem," namely the bearing capacity of a flexible strip footing at the surface of a layer of uniform weightless "undrained clay." The footing supports a uniform stress $q$, which is increased incrementally to failure. The plane strain mesh, with the out-of-plane stress included, consists of an elastic-perfectly plastic soil with a von Mises failure criterion. It should be mentioned that the trial stress can be returned to the yield surface exactly (with no iterations) for the von Mises model used in this section. The three parameter model consists of the undrained shear strength $c_u = 100\ \text{kN/m}^2$, the elastic modulus $E = 1 \times 10^5\ \text{kN/m}^2$, and Poisson's ratio $\nu = 0.3$. Theoretically, bearing failure in this problem occurs when $q$ reaches the "Prandtl load" given by

$$q_{ult} = (2 + \pi)c_u \tag{41}$$

The uniform stress $q$ versus centerline displacement by all the methods is plotted in Fig. 4. (In order to get a more meaningful plot, the large displacement given in the last step using a consistent elastoplastic modulus is omitted.) It is seen that the displacements are increasing rapidly when the load reaches 520 $\text{kN/m}^2$, indicating that bearing failure is taking place at a value very close to the "Prandtl load" of 514 $\text{kN/m}^2$. Fig. 5 shows the deformed mesh and displacement vectors at failure.

The number of iterations to achieve convergence for each load increment is shown in the first two columns of Table 1. The consistent elastoplastic modulus converges faster than the continuum one. Actually, it achieves an asymptotic quadratic convergent rate which has been recognized by Simo and Taylor (1985) and others (e.g., Keavey 2002; Asensio and Moreno 2003). It is noted that, in the algorithm described in Appendix I, the variables are updated from the converged values at the end of the previous load step. This avoids nonphysical effects such as spurious elastic unloading which can occur when path-dependent plasticity equations are driven by nonconverged values of the plastic strain. Conventionally, corrector iterations are cast in a form in which the increment is based on the difference between the current and previous iteration. It is interesting to note that when stresses are predicted based on the previous iteration, the continuum elastoplastic modulus needs fewer iterations than the consistent one. In order to demonstrate this phenomenon, the same problem was

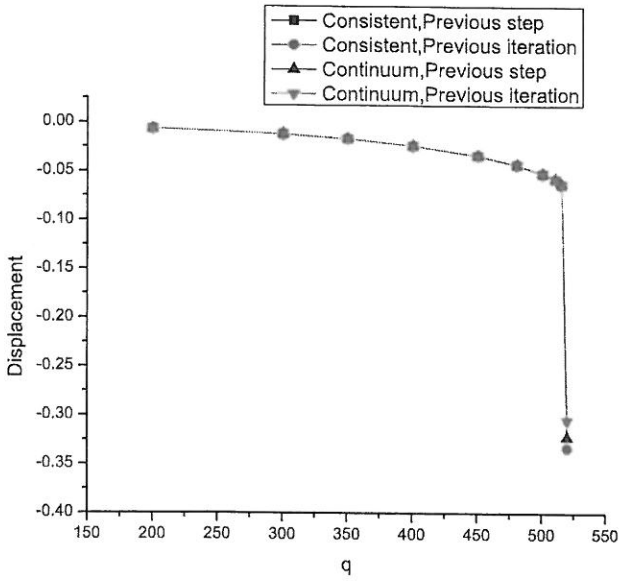


**Fig. 4.** Pressure versus centerline displacement

reanalyzed using the same algorithm except with the stresses predicted based on the previous iteration. The uniform stress $q$ versus centerline displacement using this path dependent approach are also shown in Fig. 4 and seen to be indistinguishable from the earlier results using path independent strategy. The number of iterations to achieve convergence for each load increment is shown in the last two columns of Table 1.

It can be seen in Table 1 that the continuum elastoplastic modulus needs fewer iterations than the consistent one if stresses are predicted based on the values of previous iteration. Although these stresses do not satisfy the global equilibrium equations, they still satisfy the constitutive laws. The reason why the continuum approach needs fewer iterations is that the stresses of the previous iteration are a better guess than those of previous load step.

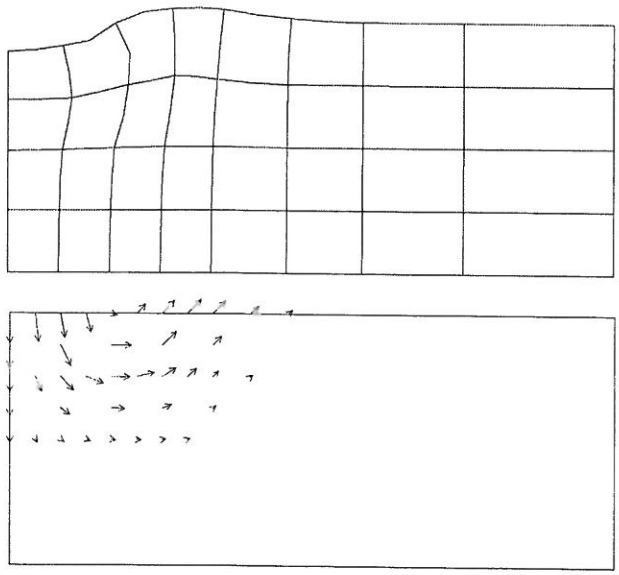

**Fig. 5.** Deformed mesh and displacement vectors at failure

**Table 1.** Number of Iterations Required by Each Method

| Step | Loads ($kN/m^2$) | Consistent previous step | Continuum previous step | Consistent previous iteration | Continuum previous iteration |
|---|---|---|---|---|---|
| 1 | 200.0 | 2 | 2 | 2 | 2 |
| 2 | 300.0 | 3 | 6 | 5 | 4 |
| 3 | 350.0 | 3 | 8 | 6 | 4 |
| 4 | 400.0 | 3 | 10 | 7 | 4 |
| 5 | 450.0 | 3 | 11 | 8 | 4 |
| 6 | 480.0 | 3 | 12 | 7 | 6 |
| 7 | 500.0 | 3 | 10 | 7 | 5 |
| 8 | 510.0 | 3 | 6 | 6 | 5 |
| 9 | 515.0 | 3 | 5 | 6 | 4 |
| 10 | 520.0 | 6 | 50 | 16 | 16 |

As pointed out by Caddemi and Martin (1991), a line search algorithm must be included to ensure convergence when CPPM is implemented with the full Newton–Raphson method. In this classical footing problem, CPPM with stresses predictions based on the previous step diverged if the load increment applied at the first step reached 460 $kN/m^2$. With the inclusion of a line search technique, however, satisfactory convergence was observed with a single step as large as 519 $kN/m^2$.

The other three algorithms described (the methods in the last three column of Table 1) can converge in response to large load steps, even when a single step approaches the ultimate value. In order to compare the influence of load step size, the same problem was analyzed using (a) a single step of 450 $kN/m^2$ and (b) five steps of 200, 100, 50, 50, 50 ($kN/m^2$) as shown in Table 1. The results are shown in Table 2 where it is seen that the consistent elastoplastic modulus with a path independent strategy had the fastest convergence rate and the continuum elastoplastic modulus with a path independent strategy, the slowest.

The ratio of the difference $r$ between the centerline displacement obtained by the two loading procedures (a) and (b) is defined as

$$r = 100 \times \left| \frac{d_a - d_b}{d_b} \right| \% \tag{42}$$

where $d_a$ and $d_b$ are the centerline displacements obtained using the two loading procedures (a) and (b), respectively. All four algorithms gave the same ultimate loads and reasonable $r$ values. The biggest difference was observed for the Continuum method based on the previous step (path independent) however even this discrepancy was less than 1.5%.

The stability of the continuum elastoplastic modulus combined a path-dependent strategy is useful when loading is conveniently applied in a single step. As for the continuum elastoplastic modulus, it can be seen from Table 1 that the path-dependent strategy needs fewer iterations than the path-independent strategy. This is a good choice when no consistent elastoplastic modulus is available. The number of iterations to convergence for all the algorithms described previously has been summarized in Table 3.

**Table 2.** Results Using Different Steps under Load of 450 $kN/m^2$

| Results | Consistent previous step | Continuum previous step | Consistent previous iteration | Continuum previous iteration |
|---|---|---|---|---|
| Iteration number (1 step) | 5 | 26 | 9 | 7 |
| $d_a$ | −0.03350 | −0.03350 | −0.03328 | −0.03263 |
| $d_b$ | −0.03321 | −0.03305 | −0.03321 | −0.03304 |
| $r\%$ | 0.87 | 1.36 | 0.21 | 1.24 |

**Table 3.** Algorithm Speed

| | Previous step | | Previous iteration |
|---|---|---|---|
| Consistent | Algorithm 1 | > | Algorithm 2 |
| | ∨ | | ∧ |
| Continuum | Algorithm 3 | < | Algorithm 4 |

## Numerical Example for CPA

### *Bearing Capacity Problem*

The stress update algorithm described in Appendix II is implemented in Program 6.5 from the open source finite-element codes of Smith and Griffiths (2004). Two types of global stiffness operators using the full Newton–Raphson method, the consistent elastoplastic modulus, and the continuum elastoplastic modulus, are considered. Although the CPA has no formal consistent elastoplastic modulus, Eq. (35) has been used leading to a pseudo-consistent approach signified by "Consistent" in the results presented later in this section. Two types of stress prediction based on the previous step and the previous iteration are also investigated. A bearing capacity problem is considered as in the previous section, however this time the soil is assumed to be frictional with a Mohr–Coulomb failure criterion. The Mohr–Coulomb failure criterion was rounded at the corners (e.g., Smith and Griffiths 2004) to avoid singularities. Several iterations were needed to return the stresses to the yield surface when trial stresses were located at the corner regions, otherwise stress updating can be carried out in one iteration. The parameters for Mohr–Coulomb are $\phi = 20°$ and $c = 15$ $kN/m^2$. The dilation angle $\psi$ is set to 20° implying as associated flow rule. The elastic parameters are $E = 1 \times 10^5$ $kN/m^2$ and $\nu = 0.3$. Theoretically, bearing failure in this problem occurs when $q$ reaches the load given by

$$q_{ult} = cN_c \tag{43}$$

where the bearing capacity factor $N_c$ is given as (Prandtl 1921)

$$N_c = \left[ \tan^2\left(45 + \frac{\phi}{2}\right) e^{\pi \tan \phi} - 1 \right] \cot \phi \tag{44}$$

For this particular case, $N_c = 14.83$ and $q_{ult} = 222.45$ $kN/m^2$.

The number of iterations to achieve convergence for each load increment is shown in Table 4. It can be seen that the "consistent" elastoplastic modulus working with path independent strategy diverged at the first load step. The other three combinations performed better and had almost the same convergence speed. It is interesting to note, as shown in Table 5, that if the load is applied in a large step, say approaching the bearing value, the continuum elastoplastic modulus working with path independent strategy has the slowest convergence properties, needing almost four times more iterations than the other two path dependent strategies. The rate of difference $r$ defined in Eq. (42) between the centerline displacement obtained by (a) one single step or (b) nine steps of 50, 50, 30, 30, 20, 20, 10, 10, 5 $kN/m^2$ to reach 225 $kN/m^2$ is also shown in Table 5. It is interesting to note that the continuum elastoplastic modulus working with stresses based on the previous

**Table 4.** Number of Iterations Required by Each Method

| Step | Loads | "Consistent" previous step | Continuum previous step | "Consistent" previous iteration | Continuum previous iteration |
|---|---|---|---|---|---|
| 1 | 50.0 | Diverged | 2 | 2 | 2 |
| 2 | 100.0 | | 6 | 7 | 7 |
| 3 | 130.0 | | 5 | 6 | 6 |
| 4 | 160.0 | | 5 | 7 | 7 |
| 5 | 180.0 | | 5 | 6 | 5 |
| 6 | 200.0 | | 5 | 8 | 7 |
| 7 | 210.0 | | 4 | 6 | 6 |
| 8 | 220.0 | | 6 | 6 | 6 |
| 9 | 225.0 | | 8 | 7 | 8 |
| 10 | 230.0 | | 50 | 50 | 50 |

step has the largest $r$. This may be the phenomenon Simo (1998) encountered. Nevertheless, all three algorithms that can converge gave the same ultimate loads as shown in Table 4.

The uniform stress $q$ versus centerline displacement of three converged algorithms is plotted in Fig. 6. It is seen that the displacements increase rapidly when the load reaches 225 kN/m$^2$, indicating that bearing failure is taking place at a value very close to the theoretical solution of $q_{ult}$=222.45 kN/m$^2$.

### Slope Stability Problem

When no consistent elastoplastic modulus is available, a path dependent strategy working with the continuum elastoplastic modulus needs fewer iterations than a path independent strategy when

**Table 5.** Results Using Different Steps under Load of 225 kN/m$^2$

| Results | "Consistent" previous step | Continuum previous step | "Consistent" previous iteration | Continuum previous iteration |
|---|---|---|---|---|
| Iteration number (1 step) | Diverged | 39 | 10 | 11 |
| $d_a$ | | −0.01312 | −0.01185 | −0.01178 |
| $d_b$ | | −0.01194 | −0.01180 | −0.01176 |
| $r$% | | 9.88 | 0.42 | 0.17 |

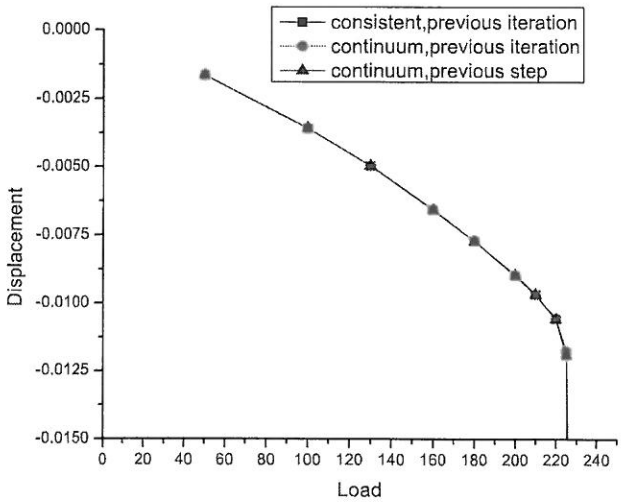


**Fig. 6.** Pressure versus centerline displacement

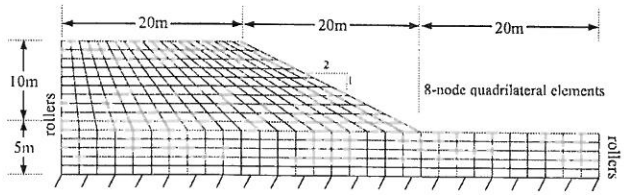


**Fig. 7.** Mesh of a slope

load is applied in a single step. Moreover, a path dependent strategy gives almost the same results when different load steps are used. Based on these observations, the following example was analyzed by CPA working with a path dependent strategy and the continuum elastoplastic modulus. The stress update algorithm described in Appendix II is implemented in Program 6.3 from the open source finite-element codes of Smith and Griffiths (2004). The problem to be analyzed is a plane strain with out-of-plane stress included slope of Mohr–Coulomb material subjected to gravity loading. The factor of safety ($FS$) of the slope is to be assessed, and this quantity is defined as the proportion by which $\tan\phi$ and $c$ must be reduced in order to cause failure under gravity loading which will be applied in a single increment. A trial strength reduction factor loop gradually weakens the soil until the algorithm fails to converge. Each entry of this loop implements a different strength reduction factor ($SRF$). The factored soil strength parameters that go into the elastoplastic analysis are obtained from

$$\phi_f = \arctan(\tan\phi/SRF)$$

$$c_f = c/SRF \tag{45}$$

Several (usually increasing) values of the $SRF$ factor are attempted until the algorithm fails to converge. The smallest value of $SRF$ to cause failure is then interpreted as the factor of safety $FS$. For a detailed description of the algorithm, the reader is referred to Griffiths and Lane (1999).

The mesh of a homogeneous 2:1 slope is displayed in Fig. 7 with $\phi$=20° and $c$=15 kN/m$^2$. The dilation angle $\psi$ is set to 20° and the unit weight is given as $\gamma$=20 kN/m$^3$. The boundary conditions are rollers on the left and right vertical boundaries, and full fixity at the base. The elastic parameters are given nominal values of $E=1\times10^5$ kN/m$^2$ and $\nu$=0.3 since they have little influence on the computed factor of safety. The convergence tolerance and iteration ceiling are set to 0.001 and 50, respectively. Six trial strength reduction factors are input, ranging from 1.0 to 1.6.

Fig. 8 gives the strength reduction factor versus the maximum nodal displacement at convergence. It can be seen that when $SRF$=1.6, the displacements increase rapidly indicating a factor of safety of about 1.6. Bishop and Morgenstern's charts (1960) give a factor of safety of 1.593 for the slope under consideration. Fig. 9 shows the deformed mesh and displacement vectors corresponding to slope failure. The mechanism of failure is clearly shown to be of the "toe" type.

To compare the efficiency of the two types of stress predictor, the problem was analyzed using the same program except with stresses prediction based on the previous load step. The results show that global iteration could not converge under $SRF$=1.4 even when the iteration ceiling was set to 3000. In this extreme case of loading applied in a single increment, it is perhaps not surprising that the path independent strategy fails, since the stresses upon which the predictions are based are all zero corresponding to an initially weightless slope.

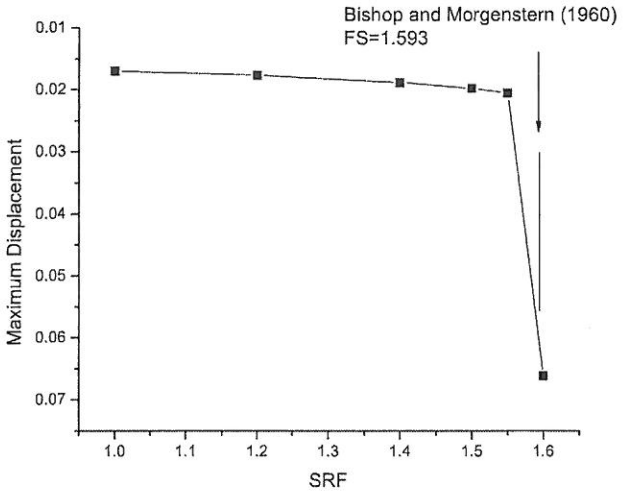


**Fig. 8.** Maximum displacement versus strength reduction factor

## Conclusion

The stability and efficiency of the CPPM and CPA return algorithms have been investigated in this paper. The algorithms have been combined with two types of stiffness operators, namely consistent and continuum elastoplastic moduli and two types of stress prediction strategies, based on stress values obtained at the previous step and stress values obtained at the previous iteration. Numerical examples show that CPPM working with a consistent elastoplastic modulus and a path independent strategy converges fastest. The significant errors for large load steps of CPA are found only when stresses are predicted based on previous steps. CPA working with a continuum elastoplastic modulus and path dependent strategy is quite stable and efficient. Moreover, both CPA itself and the continuum elastoplastic modulus avoid the need for second derivatives to be evaluated of the potential function making it easier to deal with complicated constitutive models. As for the two different stress predictors, a path dependent strategy uses a better guess to the true solution, but special care should be taken to avoid spurious elastic unloading.

## Acknowledgments

The writers gratefully acknowledge the support of the National Science Foundation's Grant No. CMS-0408150.

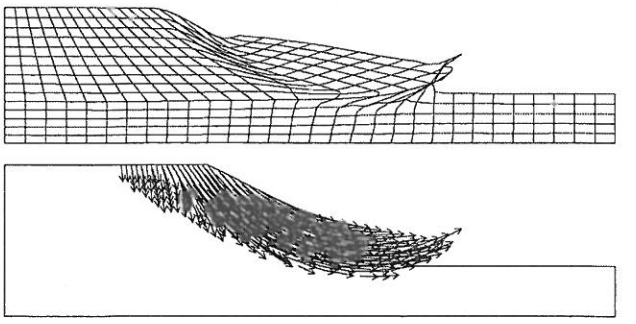

**Fig. 9.** Deformed mesh and displacement vectors at failure

## Appendix I. CPPM Iteration Procedure

1. Initialization: set initial values of plastic strain to converged values at end of previous load step, zero the incremental plasticity parameter, and evaluate the elastic trial stress

$$k=0:\ \{\varepsilon^{p(0)}\}=\{\varepsilon_n^p\},\quad \Delta\lambda^{(0)}=0,$$
$$\{\sigma^{(0)}\}=[D^e](\{\varepsilon_{n+1}\}-\{\varepsilon^{p(0)}\})$$

2. Check yield condition and convergence at $k$th iteration

$$F^{(k)}=F(\{\sigma^{(k)}\}),\quad \{r^{(k)}\}$$

If $F^{(k)}<TOL_1$ and $\|\{r^{(k)}\}\|<TOL_2$, converged else go to 3.

3. Compute increment in plasticity parameter

$$[R^{(k)}]=\left[[I]+\Delta\lambda^{(k)}[D^e]\left[\frac{\partial a^{(k)}}{\partial\sigma}\right]\right]^{-1}[D^e]$$

$$\delta\lambda^{(k)}=\frac{F^{(k)}-\{a^{(k)}\}^T[R^{(k)}]\{r^{(k)}\}}{\{a^{(k)}\}^T[R^{(k)}]\{a^{(k)}\}}$$

4. Obtain stress increments

$$\{\Delta\sigma^{(k)}\}=-[R^{(k)}]\{r^{(k)}\}-\delta\lambda^{(k)}[R^{(k)}]\{a^{(k)}\}$$

5. Update plastic strain

$$\{\varepsilon^{p(k+1)}\}=\{\varepsilon^{p(k)}\}+\{\Delta\varepsilon^{p(k)}\}=\{\varepsilon^{p(k)}\}-[D^e]^{-1}\{\Delta\sigma^{(k)}\}$$

$$\Delta\lambda^{(k+1)}=\Delta\lambda^{(k)}+\delta\lambda^{(k)}$$

$$\{\sigma^{(k+1)}\}=\{\sigma^{(k)}\}+\{\Delta\sigma^{(k)}\}$$

$$k=k+1,\quad \text{go to 2}$$

## Appendix II. CPA Iteration Procedure

1. Initialization: set initial values of plastic strain to converged values at end of previous load step, zero the incremental plasticity parameter, and evaluate the elastic trial stress

$$k=0:\ \{\varepsilon^{p(0)}\}=\{\varepsilon_n^p\},\quad \Delta\lambda^{(0)}=0,$$
$$\{\sigma^{(0)}\}=[D^e](\{\varepsilon_{n+1}\}-\{\varepsilon^{p(0)}\})$$

2. Check yield condition and convergence at $k$th iteration

$$F^{(k)}=F(\{\sigma^{(k)}\})$$

If $F^{(k)}<TOL_1$, converged else go to 3.

3. Compute increment in plasticity parameter

$$\Delta\lambda^{(k)}=\frac{F^{(k)}}{\{a^{(k)}\}^T[D^e]\{a^{(k)}\}}$$

4. Obtain stress increments

$$\{\Delta\sigma^{(k)}\}=-\Delta\lambda^{(k)}[D^e]\{a^{(k)}\}$$

5. Update plastic strain

$$\{\varepsilon^{p(k+1)}\}=\{\varepsilon^{p(k)}\}+\{\Delta\varepsilon^{p(k)}\}=\{\varepsilon^{p(k)}\}-[D^e]^{-1}\{\Delta\sigma^{(k)}\}$$

$$\{\sigma^{(k+1)}\}=\{\sigma^{(k)}\}+\{\Delta\sigma^{(k)}\}$$

$$k=k+1,\quad \text{go to 2}$$

## Notation

*The following symbols are used in this paper:*

$\{a\}$ = gradient of yield function or plastic potential function respect to stresses;
$c$ = cohesion;
$[D^e]$ = elastic stress-strain tensor;
$[D^{ep}]$ = continuum elastoplastic modulus;
$\{D^{epc}\}$ = consistent elastoplastic modulus;
$E$ = Young's modulus;
$F$ = yield function;
$k$ = iteration counter;
$N_c$ = bearing capacity factor;
$n$ = load step counter;
$q_{ult}$ = bearing capacity;
$\{\Delta\varepsilon\}$ = total strain increment;
$\{\varepsilon\}$ = strain;
$\{\dot{\varepsilon}\}$ = strain rate;
$\{\dot{\varepsilon}^e\}$ = elastic component of strain rate;
$\{\dot{\varepsilon}^p\}$ = plastic component of strain rate;
$\dot{\lambda}$ = consistency parameter;
$\nu$ = Poisson's ratio;
$\{\sigma\}$ = stress;
$\{\dot{\sigma}\}$ = stress rate;
$\{\sigma^{trial}\}$ = trial stress;
$\phi$ = friction angle; and
$\psi$ = dilation angle.

## References


Armero, F., and Pérez-Foguet, A. (2002). "On the formulation of closest-point projection algorithms in elastoplasticity. Part I: The variational structure." *Int. J. Numer. Methods Eng.*, 53(2), 297–329.

Asensio, G., and Moreno, C. (2003). "Linearization and return mapping algorithms for elastoplasticity models." *Int. J. Numer. Methods Eng.*, 57(7), 991–1014.

Belytschko, T., Liu, W. K., and Moran, B. (2000). *Nonlinear finite elements for continua and structures*, Wiley, England, 278–286.

Bićanić, N., and Pearce, C. J. (1996). "Computational aspects of a softening plasticity model for plain concrete." *Mech. Cohesive-Frict. Mater.*, 1(1), 75–94.

Bishop, A. W., and Morgenstern, N. R. (1960). "Stability coefficients for earth slopes." *Geotechnique*, 10(4), 129–150.

Borja, R. I., Sama, K. M., and Sanz, P. F. (2003). "On the numerical integration of three-invariant elastoplastic constitutive models." *Comput. Methods Appl. Mech. Eng.*, 192(9–10), 1227–1258.

Caddemi, S., and Martin, J. B. (1991). "Convergence of the Newton–Raphson algorithm in elastic-plastic incremental analysis." *Int. J. Numer. Methods Eng.*, 31(1), 177–191.

Clausen, J., Damkilde, L., and Andersen, L. (2006). "Efficient return algorithms for associated plasticity with multiple yield planes." *Int. J. Numer. Methods Eng.*, 66(6), 1036–1059.

Crisfield, M. A. (1991). *Non-linear finite element analysis of solids and structures*, Vol. 1, Wiley, N.Y.

Crisfield, M. A. (1997). *Non-linear finite element analysis of solids and structures, Advanced topics*, Vol. 2, Wiley, N.Y.

de Borst, R. (1987). "Integration of plasticity equations for singular yield functions." *Comput. Struct.*, 26(5), 823–829.

de Souza Neto, E. A., Perić, D., and Owen, D. R. J. (1994). "A model for elastoplastic damage at finite strains: Algorithmic issues and applications." *Eng. Comput.*, 11(3), 257–281.

Griffiths, D. V., and Lane, P. A. (1999). "Slope stability analysis by finite elements." *Geotechnique*, 49(3), 387–403.

Huang, J., and Griffiths, D. V. (2008). "Observations on return mapping algorithms for piecewise linear yield criteria." *Int. J. Geomech.*, 8(4), 253–265.

Hughes, T. J. R., and Pister, K. S. (1978). "Consistent linearization in mechanics of solids and structures." *Comput. Struct.*, 9(3–4), 391–397.

Hughes, T. J. R., and Taylor, R. L. (1978). "Unconditionally stable algorithms for quasi-static elasto/viscoplastic finite element analysis." *Comput. Struct.*, 8(2), 169–173.

Jeremić, B. (2001). "Line search techniques for elasto-plastic finite element computations in geomechanics." *Commun. Numer. Methods Eng.*, 17(2), 115–125.

Jirasek, M., and Bažant, Z. P. (2001). *Inelastic analysis of structures*, Wiley, N.Y.

Keavey, M. A. (2002). "A canonical form return mapping algorithm for rate independent plasticity." *Int. J. Numer. Methods Eng.*, 53(6), 1491–1510.

Koiter, W. T. (1953). "Stress-strain relations, uniqueness and variational theorems for elastic-plastic materials with a singular yield surface." *Q. Appl. Math.*, 11, 350–354.

Krieg, R. D., and Krieg, D. B. (1977). "Accuracies of numerical solution methods for the elastic-perfectly plastic model." *ASME J. Pressure Vessel Technol.*, 99(4), 510–515.

Larsson, R., and Runesson, K. (1996). "Implicit integration and consistent linearization for yield criteria of the Mohr–Coulomb type." *Mech. Cohesive-Frict. Mater.*, 1(4), 367–383.

Masud, A., and Xia, K. (2005). "A stabilized mixed finite element method for nearly incompressible elasticity." *J. Appl. Mech.*, 72(5), 711–720.

Nayak, G. C., and Zienkiewicz, O. C. (1972). "Elastic-plastic stress analysis: A generalisation for various constitutive relations including strain softening." *Int. J. Numer. Methods Eng.*, 5(1), 113–135.

Ortiz, M., and Popov, E. P. (1985). "Accuracy and stability of integration algorithms for elastoplastic constitutive relations." *Int. J. Numer. Methods Eng.*, 21(9), 1561–1576.

Ortiz, M., and Simo, J. C. (1986). "An analysis of a new class of integration algorithms for elastoplastic constitutive relations." *Int. J. Numer. Methods Eng.*, 23(3), 353–366.

Owen, D. J. R., and Hinton, E. F. (1980). *Finite element in plasticity: Theory and practice*, Pineridge Press, Swansea.

Pérez-Foguet, A., and Armero, F. (2002). "On the formulation of closest-point projection algorithms in elastoplasticity. Part II: Globally convergent schemes (with application to deviatoric and pressure-dependent plastic models)." *Int. J. Numer. Methods Eng.*, 53(2), 331–374.

Péréz-Foguet, A., Rodríguez-Ferran, A., and Huerta, A. (2001). "Consistent tangent matrices for substepping schemes." *Comput. Methods Appl. Mech. Eng.*, 190(35–36), 4627–4647.

Prandtl, L. (1921). "über die Eindringungsfestigkeit (Härte) plastischer Baustoffe und die Festigkeit von Schneiden." *Z. Angew. Math. Mech.*, 1, 15–20.

Simo, J. C. (1998). "Numerical analysis of classical plasticity." *Handbook for numerical analysis*, P. G. Ciarlet and J. J. Lions, eds., Vol. VI, Elsevier, Amsterdam.

Simo, J. C., and Hughes, T. J. R. (1998). *Computational inelasticity*, Springer, N.Y.

Simo, J. C., and Ortiz, M. A. (1985). "A unified approach to finite deformation elastoplastic analysis based on the use of hyperelastic constitutive-equations." *Comput. Methods Appl. Mech. Eng.*, 49(2), 221–245.

Simo, J. C., and Taylor, R. L. (1985). "Consistent tangent operators for rate-independent elastoplasticity." *Comput. Methods Appl. Mech. Eng.*, 48(3), 101–118.

Smith, I. M., and Griffiths, D. V. (2004). *Programming the finite element method*, 4th Ed., Wiley, N.Y.

Xia, K., and Masud, A. (2006). "New stabilized finite element method embedded with a cap model for the analysis of granular materials." *J. Eng. Mech.*, 132(3), 250–259.

Zienkiewicz, O. C., Valliapan, S., and King, I. P. (1969). "Elasto-plastic solutions of engineering problems—The initial stress finite element approach." *Int. J. Numer. Methods Eng.*, 1(1), 75–100.